ELSEVIER

Cell Calcium xxx (2007) xxx–xxx

cell calcium

www.elsevier.com/locate/ceca

Multi-dimensional resolution of elementary Ca^{2+} signals by simultaneous multi-focal imaging

Angelo Demuro [a,*], Ian Parker [a,b]

[a] *Department of Neurobiology & Behavior, University of California, Irvine, CA 92697, United States*
[b] *Department of Physiology & Biophysics, University of California, Irvine, CA 92697, United States*

Received 4 December 2006; received in revised form 30 June 2007; accepted 6 July 2007

Abstract

Elementary events such as puffs and sparks are cytosolic microdomains of Ca^{2+} from which cellular Ca^{2+} signals are constructed. Because of the tight localization and fast kinetics of elementary events, imaging studies have been hindered by instrumental limitations of confocal and deconvolution fluorescence microscopy which necessitate compromises between spatial and temporal resolution. Here, we describe a novel, yet simple 'multi-focal' fluorescence microscopy system that employs three high-speed cameras focused at different axial depths to enable 4-dimensional imaging with millisecond resolution. We demonstrate the utility of this system for studies of puffs in *Xenopus* oocytes by mapping the axial distribution of puff sites, by obtaining measurements of puff amplitudes undistorted by focus error, and by deriving deblurred images that reveal novel sub-micron jumps of Ca^{2+} release sites.
Published by Elsevier Ltd.

Keywords: Ca^{2+} puffs; Multi-focal imaging; Ca^{2+} imaging

1. Introduction

'Elementary' Ca^{2+} signals are local, transient elevations of cytosolic Ca^{2+} that arise through liberation of Ca^{2+} from the endoplasmic reticulum [1]. Examples include Ca^{2+} puffs and sparks, which are mediated, respectively, by inositol trisphosphate receptors (IP_3R) and ryanodine receptors (RyR) [1–4]. In both cases, Ca^{2+} liberation is believed to occur through several tightly clustered receptor/channels, whose opening is coordinated by a process of Ca^{2+}-induced-Ca^{2+} release. Elementary Ca^{2+} transients are a ubiquitous signaling mechanism across a wide variety of cell types, and they serve both as the building blocks from which global cellular signals are constructed and as local signals in their own right [1]. Given their importance for regulating cellular functions as diverse as cardiac contraction and neuronal excitability it is important to understand the fundamental mechanisms underlying the generation of puffs and sparks. However, crucial questions remain unanswered; including the numbers and spatial distribution of the Ca^{2+} release channels, and the mechanism causing termination of Ca^{2+} release.

A major difficulty in studying elementary Ca^{2+} signals arises from their rapid kinetics (ca. 10 ms for sparks, a few tens of ms for puffs) and tight spatial localization (<2 μm). Most studies have utilized confocal techniques to image Ca^{2+} signals reported by fluorescent indicator dyes, because the optical 'sectioning' effect generated by this technique provides good (ca. 600 nm) axial spatial resolution. However, construction of an image requires raster-scanning the laser spot, a time-consuming process that necessitates a trade-off between temporal and spatial information. Indeed, in order

Abbreviations: IP_3, inositol 1,4,5-triphosphate; IP_3R, inositol 1,4,5-triphosphate receptor; RyR, ryanodine receptor

* Corresponding author. Tel.: +1 949 824 7833; fax: +1 949 824 2447.
E-mail address: ademuro@uci.edu (A. Demuro).

0143-4160/$ – see front matter. Published by Elsevier Ltd.
doi:10.1016/j.ceca.2007.07.002

Please cite this article in press as: A. Demuro, I. Parker, Multi-dimensional resolution of elementary Ca^{2+} signals by simultaneous multi-focal imaging, Cell Calc. (2007), doi:10.1016/j.ceca.2007.07.002

to adequately track the kinetics of puffs and sparks, spatial information is often sacrificed to the extent that only a single dimension is acquired. That is to say, the laser is repeatedly scanned along a single line to derive a linescan image representing the temporal evolution of Ca^{2+} signals in one spatial dimension [5]. Although widely used, confocal linescan imaging suffers a serious limitation in that there is no definitive way of knowing whether a particular Ca^{2+} event was focal (i.e. that it arose at a site directly intersected by the scan line), or whether the fluorescence signal arose from Ca^{2+} diffusing from a remote site displaced laterally and/or axially (in *y* or *z* dimensions) from the scan line. Such non-focal fluorescence signals are of smaller amplitude and slower time course as compared to focal signals, and theoretical models show that this distortion makes it impossible to obtain an accurate distribution of event amplitudes [6]. For example, even if Ca^{2+} sparks were identical, the random placement of the scan line predicts a broad distribution of observed spark amplitudes [7].

An alternative approach involves 'wide-field' fluorescence imaging with a high-speed camera [8,9]. This provides well-resolved two-dimensional (*x*–*y*) spatial information, and the latest generation of electron-multiplied or intensified CCD cameras are capable of imaging at rates of several hundred frames per second or better. The major drawback, however, is that – unlike the sectioning achieved by confocal microscopy – wide-field imaging provides little axial (*z*) resolution. Thus, fluorescence events originating above or below the plane of focus appear strongly blurred, but contribute almost the same total fluorescence across the imaging field as equivalent in-focus events [9,10]. In principle, this drawback can be largely mitigated by acquiring a stack of images acquired sequentially with the microscope focused at progressive increments along the *z*-axis. The axial position of an event can then be determined from the plane where it appears most sharply in focus [8], and deconvolution techniques can be applied to reduce blurring [11]. Such approaches work well for static specimens, but are problematic for dynamic imaging of fast events such as local Ca^{2+} microdomains when the signal may change appreciably during the time required to step between and acquire sequential image planes. The acquisition rate is necessarily constrained both by the camera frame rate and by mechanical inertia that limits the speed at which the microscope can be focused. By use of a custom CCD camera and piezoelectric objective translator, Kirber et al. [8] were able to collect 3D data sets of five image planes as fast as every 26.5 ms. Nevertheless, that remains slow in comparison to the rise times of puffs and sparks.

Here, we describe a new approach to fast time-resolved 3D imaging of elementary Ca^{2+} signals, involving simultaneous imaging with three high-speed cameras, each focused at a different plane in the specimen. We illustrate the use of this simple technique to image Ca^{2+} puffs in *Xenopus* oocytes by mapping their axial distribution and by estimating their amplitudes undistorted by focus error. Furthermore, we derived deblurred images that reveal novel sub-micron jumps of Ca^{2+} between release sites.

2. Materials and methods

2.1. Multi-focal imaging system

The imaging system illustrated schematically in Fig. 1A was constructed from three identical Cascade 128+ cameras (Roper Scientific) mounted on a small (1 ft × 1 ft) optical breadboard attached to the side port of an Olympus IX 71 inverted microscope. A diverging lens (L1) mounted on the side port window extended the microscope image plane to a position 23 cm from the microscope body, thereby allowing sufficient space to mount the three cameras. The fluorescence signal from the microscope was divided by two plate beam-splitters (BS1; 30% reflectance, 70% transmission: and BS2; 50/50% reflection/transmission) so as to form images of roughly equal brightness on the sensor chips of the three cameras. The beam-splitters were fixed on high-precision adjustable mounts, so that the images on the two cameras receiving reflected light (*Cam1* and *Cam3*) could be aligned laterally (*x*–*y*) with that formed by the central camera (*Cam2*) receiving transmitted light. Correct alignment was achieved by imaging fluorescent beads (100 nm diameter; 'fluospheres', Invitrogen), and adjusting the beam splitters to bring the three images into register when viewed as a color-composite on the computer monitor. Each camera was mounted on a single-axis translation stage, permitting fine movement along the optical (*z*) axis. *Cam2* was adjusted to be parafocal with the microscope image as viewed through the oculars. *Cam1* and *Cam3* were, respectively, adjusted so as to focus at equal increments (usually 2 μm for Ca^{2+} imaging) more deeply and more superficially into the specimen than *Cam2*. The focus difference was calibrated by measuring the displacement of the microscope focus knob required to bring the image of a fluorescent bead into focus for each camera. Because the differential focusing between the cameras was achieved by varying the back focal length rather than by refocusing the objective, the effective magnification for each camera varied slightly, thereby introducing an offset for objects away from the central axis. However, this misregistration was negligible for the focal spacings (generally ≤2 μm) used here, amounting to <1 pixel even at the corners generally of the camera field.

The microscope was equipped with a 40× NA 1.35 oil immersion objective, and a standard FITC cube for wide-field epifluorescence imaging. Excitation light was provided by a 488 nm, 100 mW argon ion laser, with emitted fluorescence collected through a 500 nm dichroic mirror and a 510 nm long-pass barrier filter. The microscope was further modified by addition of a second dichroic mirror before the objective, to allow delivery of flashes of UV light (350–400 nm) from an Hg arc lamp for photolysis of caged IP_3.

The Cascade 128+ cameras incorporated a cooled, back-illuminated CCD sensor with on-chip electron multiplication. This provided high (>0.8) quantum efficiency, together with effectively negligible read-out and dark noise, at a maximum frame rate of ∼500 s^{-1} for full (128 × 128 pixel) resolu-

Please cite this article in press as: A. Demuro, I. Parker, Multi-dimensional resolution of elementary Ca^{2+} signals by simultaneous multi-focal imaging, Cell Calc. (2007), doi:10.1016/j.ceca.2007.07.002

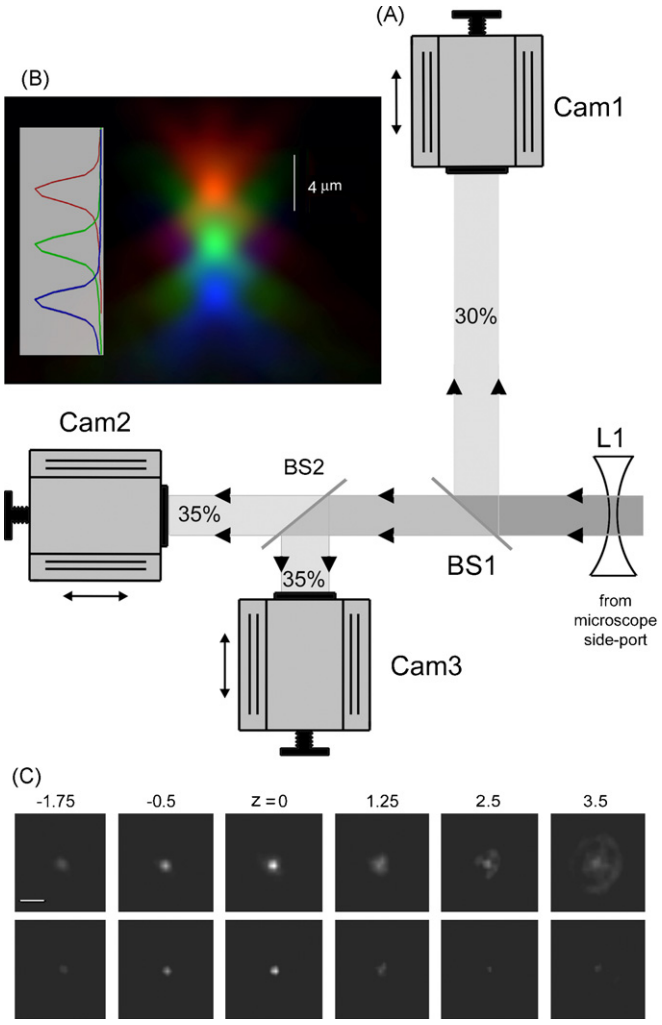

Fig. 1. Simultaneous multi-focal imaging system. (A) Schematic of the triple-camera system, constructed on an optical breadboard located at the side-port of an Olympus IX 71 inverted microscope. *Cam1*, *Cam2* and *Cam3* are identical Cascade 128+ cameras, each mounted on single-axis translation stages allowing their distances from the focal plane of the microscope to be independently varied. BS1 is a beam splitter that reflects 30% of the emitted fluorescence light toward *Cam1*. The remaining light is then divided equally between *Cam2* and *Cam3* by BS2, a beam splitter with 50/50 transmission/reflection. Both beam splitters are fixed on adjustable mirror mounts allowing fine alignment of tilt in *x* and *y*-axes to superimpose the images formed by the three cameras. The diagram is not to scale, and differences in path lengths for the cameras are exaggerated for clarity. (B) Axial (*x*–*z*) point-spread functions (p.s.f.) for the three individual cameras (pseudocolored in red, green and blue) obtained by focusing through a sub-resolution (100 nm) fluorescent bead. (C) Enhancement of the microscope p.s.f. by applying a 'deblurring' algorithm to images from the three cameras. The upper row shows selected frames from the center camera while focusing through a 100 nm fluorescent bead embedded in agarose. The lower row shows corresponding images after correction for out-of-focus fluorescence by subtracting smoothed (15 × 15 pixels), averaged images acquired at focal planes 250 nm above and below the center camera. Axial depths are indicated in μm relative to the bead. Calibration bar = 1 μm.

tion. The magnification corresponded to 0.29 μm per pixel. Signals from the cameras were acquired simultaneously by three PCI interface cards in a PC running V++, with synchronization between the cameras maintained to better than 1 ms throughout recordings as long as 30 s.

2.2. Image processing

Image streams were saved as multi-image TIFF files, and imported into MetaMorph (Molecular Dynamics) for off-line processing and analysis. After black level subtraction, image streams from the three cameras were each divided by the respective background fluorescence images (obtained by averaging 50 frames before flash stimulation) to obtain fluorescence pseudo-ratio ($\Delta F/F_0$) images. The images in Figs. 2 and 5 were further processed by pixel interpolation to smooth out the 'blocky' pixellated appearance resulting from the relatively coarse (128 × 128) resolution of the camera by zooming by 4× and smoothing the result by a 12 × 12 pixel filter. Finally, the *Cam2* images were 'deblurred' by frame-by-frame subtraction of a smoothed (19 × 19 interpolated pixel filter) average of *Cam1* + *Cam3* images.

2.3. Imaging 'model' Ca^{2+} puffs

To test and validate the principle of our multi-focal system, we imaged sub-resolution (100 nm) fluorescent beads and 'model' Ca^{2+} puffs generated by ionophoresis of Ca^{2+} from a sharp micropipette. Ca^{2+} injections were made into Ringer's solution containing 4 μM Fluo-4-dextran, 500 μM EGTA with no added Ca^{2+} and 5% Ficol (to increase viscosity and thereby slow Ca^{2+} diffusion). A backing current was applied to prevent Ca^{2+} leakage from the pipette, and ionophoretic pulses (20 ms duration; 1–5 nA) were adjusted to evoke fluorescence signals with amplitudes and kinetics roughly comparable to puffs in the oocyte. Fluorescence signals evoked by repeated ionophoretic pulses (at 500 ms intervals) were highly reproducible and, because we had three cameras available for only a short time, data presented in Figs. 1C and 2 were simulated by manually re-focusing a single camera at successive planes.

2.4. Oocyte preparation and injection

Experiments were performed on defolliculated stage V and VI oocytes obtained from *Xenopus laevis* [12]. About 30 min–2 h before use these were injected with 40 nl of an aqueous solution containing 2 mM fluo-4-dextran (MW 10,000 D; low-affinity version, K_D for Ca^{2+} about 3 μM), 0.4 mM caged IP_3, and 6 mM EGTA, resulting in final intracellular concentrations of roughly 40, 16 and 240 μM. Oocytes were then placed animal hemisphere-down in a chamber whose base was formed by a fresh microscope cover glass (Fisherbrand, type-545-M), and were bathed in Ringer's

Please cite this article in press as: A. Demuro, I. Parker, Multi-dimensional resolution of elementary Ca^{2+} signals by simultaneous multi-focal imaging, Cell Calc. (2007), doi:10.1016/j.ceca.2007.07.002

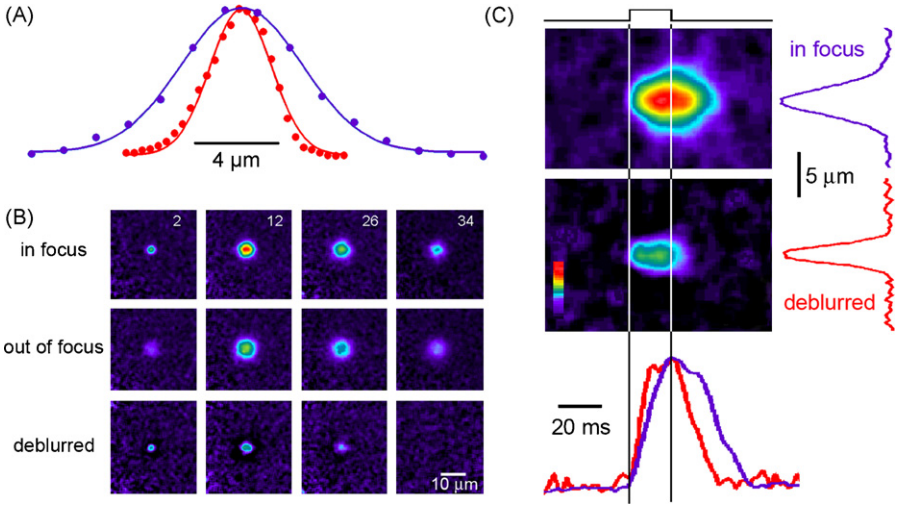

Fig. 2. Multi-focal imaging of 'model' Ca^{2+} puffs evoked by ionophoresis of Ca^{2+} from a micropipette into a solution of indicator dye. (A) Comparison of the axial p.s.f. of the microscope derived using a sub-resolution fluorescent bead (red curve) with the axial distribution of fluorescence resulting from diffusional spread of Ca^{2+} from the tip of the ionophoretic pipette (purple curve). (B) Selected frames captured at different times during and after an ionophoretic Ca^{2+} pulse. The top sequence was obtained from a plane focused on the pipette tip, and the middle sequence from a plane 4 μm below. Numbers in the top frames indicate time (in ms) following onset of the 20 ms duration ionophoretic pulse. The lower sequence shows corresponding images after applying the 'deblurring' algorithm (see text) to correct for out-of-focus fluorescence. (C) Line-scan (*x–t*) images derived from the full image sequences in B, show the fluorescence signals from the model puff before (top image) and after (bottom image) deblurring. Traces at the right show corresponding spatial profiles of fluorescence measured at the time of peak response, and the traces at the bottom show corresponding temporal profiles measured at the location of the pipette tip. Purple traces were obtained from linescan images of the raw in-focus signal, and red traces from the deblurred signal. The duration of the ionophoretic Ca^{2+} pulse is indicated by the vertical lines. Amplitudes are normalized to facilitate comparison. Fluorescence intensities in B and C are depicted on a blue-red pseudocolor scale, uniform for all images, with red corresponding to the brightest signal in the in-focus images.

solution (composition in mM: NaCl, 110; $CaCl_2$, 2, KCl, 2; HEPES, 5; at pH 7.2.).

3. Results and discussion

3.1. Point-spread function and validation of the multi-focal imaging system

To align and test the system we imaged 100 nm fluorescent beads suspended in an agarose gel. Fig. 1B shows the axial point-spread function (p.s.f.) of the three-camera system as a pseudocolor montage, overlaying *x–z* images from each camera obtained by focusing the microscope in 0.25 μm steps through a bead. Fig. 1C further shows the substantial improvement in p.s.f. achieved by a simple 'deblurring' algorithm as described in Section 2.2, whereby out-of-focus fluorescence in the in-focus image plane was reduced by subtracting an average of smoothed images acquired at planes above and below the focal plane. In this instance we sought to correct for the diffraction-limited blurring of the microscope and accordingly acquired from triplet image planes spaced 0.25 μm apart, whereas a 2 μm spacing was used to correct for the greater diffusional blurring of Ca^{2+} signals.

We then explored the potential of multi-focal imaging for resolution of fast, dynamic Ca^{2+} signals, employing a model system where ionophoretic pulses of Ca^{2+} into an aqueous solution of indicator dye were used to image the diffusional spread of Ca^{2+} from a point source. Fig. 2A (purple curve) shows the axial distribution of resulting fluorescence, measured from the central camera just before the end of the ionophoretic pulse. This is well fitted by a Gaussian distribution and, as expected, the axial distribution is appreciably wider than that of a sub-resolution bead (red curve, Fig. 2A), because it reflects the diffusional spread of Ca^{2+} and Ca^{2+}-bound indicator in addition to the microscope p.s.f. A major rationale prompting our construction of a multi-focal imaging system was to compensate for this 'diffusional blurring' effect as well as the optical blurring of the microscope, so as to more precisely locate the source and kinetics of the Ca^{2+} release flux underlying local Ca^{2+} signals such as puffs. Application of this process is illustrated in Fig. 2B, showing the temporal evolution of a 'model Ca^{2+} puff' generated by ionophoresis of Ca^{2+} into indicator solution. The upper row of images was obtained with the focus on the tip of the ionophoretic pipette, and the middle images from a plane 4 μm below. The bottom image sequence was derived using the 'deblurring' algorithm, and shows clear enhancements in terms of temporal dynamics and tighter localization of the Ca^{2+} source. These improvements are further highlighted in Fig. 2C, showing line-scan (*x–t*) images derived from the full *x–y* image sequences by measuring fluorescence along a line passing through the location of the pipette tip. The radial spread of the 'deblurred' fluorescence signal is appreciably narrower than that of the 'raw' in-focus signal; localization of the Ca^{2+} source is facilitated, and the kinetics of the

Please cite this article in press as: A. Demuro, I. Parker, Multi-dimensional resolution of elementary Ca^{2+} signals by simultaneous multi-focal imaging, Cell Calc. (2007), doi:10.1016/j.ceca.2007.07.002

'deblurred' signal match more closely the duration for which the ionophoretic pulse was applied.

3.2. High speed imaging of Ca^{2+} puffs

To establish the utility of the multi-focal microscope for study of local, intracellular Ca^{2+} signals, we imaged Ca^{2+} puffs in *Xenopus* oocytes by epifluorescence microscopy using three Cascade 128+ cameras operating at 500 or 200 frames s^{-1}. Flashes of UV light were applied to photorelease IP_3, resulting in stochastic triggering of puffs at numerous locations within the imaging field (40 μm × 40 μm; 128 × 128 pixels) following latencies of tens of ms to a few s. In these experiments, oocytes were injected with the slow Ca^{2+} buffer EGTA to a cytosolic concentration of ~240 μM, which functionally uncouples puff sites and inhibits Ca^{2+} waves by impairing long-range Ca^{2+}-induced Ca^{2+} release between sites without appreciably affecting the magnitude or kinetics of the puffs themselves [13,14].

Fig. 3A shows examples of puffs captured by the central camera (*Cam 2*) at different times following photorelease of IP_3. Several puffs are evident, originating at different sites.

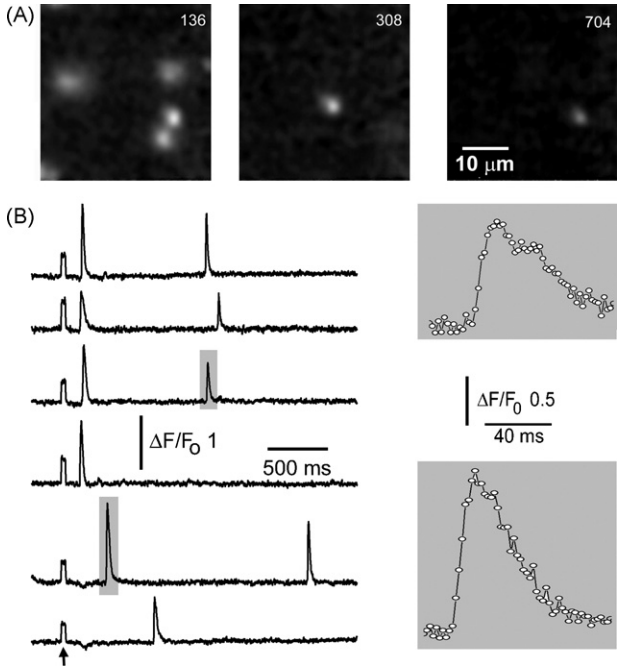

Fig. 3. Time-resolved imaging of IP_3-evoked Ca^{2+} puffs in *Xenopus* oocytes. (A) Representative single frames (a few hundred ms apart) taken from a sequence acquired at 2 ms intervals show fluorescence ratio changes ($\Delta F/F_0$) of the calcium indicator fluo-4 imaged by *Cam2*. A flash of UV light (arrow marks flash artifact) uniformly illuminating the imaging field was applied 1 s before the first image to photoreleased IP_3, resulting in Ca^{2+} puffs at multiple locations after variable latencies. (B) Traces illustrate the fast kinetics of puffs, monitored simultaneously at 2 sites from (1.2 μm × 1.2 μm) regions of interest on the *Cam2* image. The puffs indicated by shaded boxes are shown on an expanded time scale on the right. Data points are at 2 ms frame intervals.

Some appear sharply resolved, whereas others are out of focus in this plane. Puff kinetics were resolved by measuring Ca^{2+}-dependent fluorescence from small regions of interest centered on puff sites (Fig. 3B). Many sites showed only a single puff following the flash, but others showed two events a few seconds apart. The insets in Fig. 3B show examples of puffs on an expanded timescale. These show rise times of <10 ms—sufficiently rapid as to defeat attempts at 3D (*x*,*y*,*z*) imaging by acquiring sequential *z*-planes even at frame rates as fast as 500 s^{-1}.

3.3. Simultaneous x–y–z imaging of puffs

Multi-focal imaging allowed us to circumvent the above limitation by simultaneously acquiring images at three focal planes. For example, the inset traces in Fig. 4A show a single puff monitored from the same region of interest in the three image sequences. In this instance the largest signal was obtained from *Cam1*, indicating that the puff site probably lay close to the focal depth of that camera and deeper into the oocyte than the focal planes of *Cam2* and *Cam3*. Other puffs at different lateral locations in the same image sequence showed varying distributions in amplitudes between the three cameras: for example, Fig. 4B shows a puff arising at a depth close to the focal plane of *Cam2*, and Fig. 4C shows a puff at a depth intermediate between *Cam2* and *Cam3*.

3.4. Axial locations of puff sites

To obtain a more quantitative estimate of the depth of puff sites we then plotted the peak puff amplitude as a function of focal plane of each camera (dots in graphs of Fig. 4A–C). Measurements of puff amplitudes at three depths provide (just) sufficient information to fit a Gaussian curve with free parameters of amplitude, center position (i.e. axial depth of the puff site) and standard deviation (width). The axial width was allowed to vary as required to obtain the best fit to each event. To estimate the precision with which axial puff locations could be determined, we examined the differences between paired measurements at sites that showed two puffs in response to a photolysis flash, assuming that both puffs arose at identical sites. The standard deviation of the difference in axial position of paired events was 0.37 μm ($n = 29$ puff sites).

Fig. 4D shows the distribution of axial depths of puff sites as estimated from 110 events by determining the center position of Gaussian fits as in Fig. 4A–C. Depths are referenced to the focal plane of *Cam2*, which was focused by eye at the level of the pigment granules in the oocyte. Almost all puffs arose within a thin band about 5 μm wide, centered close to the granule layer: results that are in close agreement with those obtained previously by use of axial linescan confocal microscopy [5].

Please cite this article in press as: A. Demuro, I. Parker, Multi-dimensional resolution of elementary Ca^{2+} signals by simultaneous multi-focal imaging, Cell Calc. (2007), doi:10.1016/j.ceca.2007.07.002

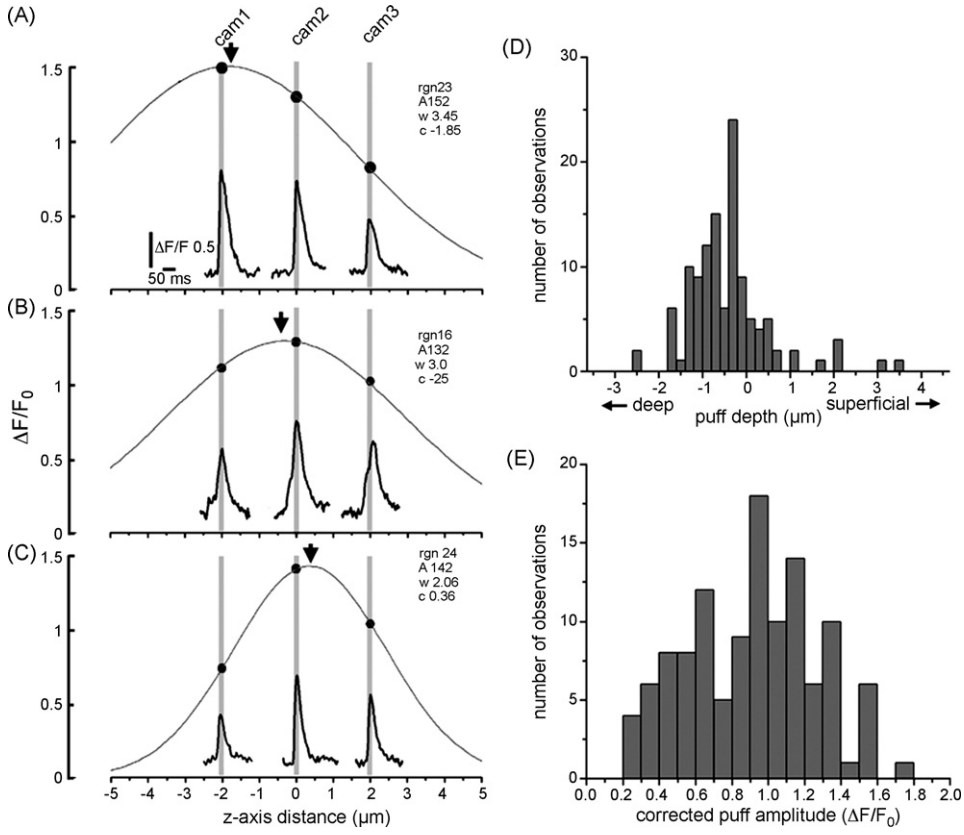

Fig. 4. Axial localization and amplitude correction of puffs by multi-focal imaging. (A) Example of a single puff imaged simultaneously by the three cameras (*Cam1*, *Cam2*, *Cam3*) focused at 2 μm increments in the *z*-axis. Inset traces show fluorescence ratio changes monitored from identical small (1.2 μm square) regions of interest in the image sequences captured by each camera. The main graph plots the peak puff magnitude as a function of the axial displacement of the focal planes in the specimen relative to *Cam2*. The smooth curve is a Gaussian fit to the data. In this instance, the greatest puff amplitude was recorded by *Cam1*, indicating that the puff arose at a depth in the oocyte (peak of Gaussian marked by arrow) close to the focus of that camera. (B and C) Corresponding examples of puffs that originated at differing axial depths. (D) Axial distribution of puff sites in the oocyte. The histogram shows the numbers of observed puff sites as a function of depth as determined from the peaks of Gaussian fits as illustrated in A–C. Depths are referenced to the object plane of *Cam2*, which was focused by eye at the level of the thin shell of pigment granules in the oocyte. (E) Distribution of peak puff amplitudes obtained after correcting for distortion by out-of-focus events. For each puff, the amplitude was taken as the peak amplitude of a Gaussian fit to the 'raw' amplitude data derived from the three cameras, as illustrated in A–C. Data in D and E are derived from measurements of 110 puffs.

3.5. *Puff amplitudes*

The "raw" fluorescence signals measured from small regions of interest in images obtained by widefield or confocal microscopy underestimate the 'true' amplitudes of puffs unless the puff sites happen by chance to lie at the focal plane. This is readily apparent in Fig. 4A–C, where 2 μm focus displacements result in nearly 50% changes in fluorescence amplitude; and the error would likely be even greater with confocal sectioning. To compensate for this distortion, we derived corrected puff amplitudes from the peaks of Gaussian curves fitted to simultaneous measurements from the three cameras. The distribution of corrected fluorescence ratio amplitudes from 110 events is plotted in Fig. 4E. This shows a broad (~8-fold) range; validating previous conclusions that puffs show a wide variability in Ca^{2+} release fluxes [15,16]. However, it is likely that those earlier measurements obtained by confocal microscopy would be subject to further variability owing to inclusion of out-of-focus events. An important advantage of multi-focal imaging is that it allows unambiguous selection of events that lie at depths between the focal planes of *Cam1* and *Cam3* where accurate determination of amplitudes is possible. In contrast, selection of events from confocal images is based largely on arbitrary and subjective criteria to exclude out-of-focus events on the basis of small and/or diffuse signals.

3.6. *'Calcium deblurring' of multi-focal puff images*

As illustrated with the 'model' puff in Fig. 2, simultaneous acquisition at adjacent *z*-planes enables us to 'deblurr' images so as to partially compensate for diffusion of Ca^{2+} and out-of-focus fluorescence. Fig. 5 illustrates the application of this approach to IP_3-evoked puffs in the oocyte, which helps reveal novel features of puff micro-architecture. We employed a simple algorithm involving subtraction of a smoothed average of the outer *Cam1* + *Cam3* images from the center *Cam2* image for selected puffs that were in focus on

Please cite this article in press as: A. Demuro, I. Parker, Multi-dimensional resolution of elementary Ca^{2+} signals by simultaneous multi-focal imaging, Cell Calc. (2007), doi:10.1016/j.ceca.2007.07.002

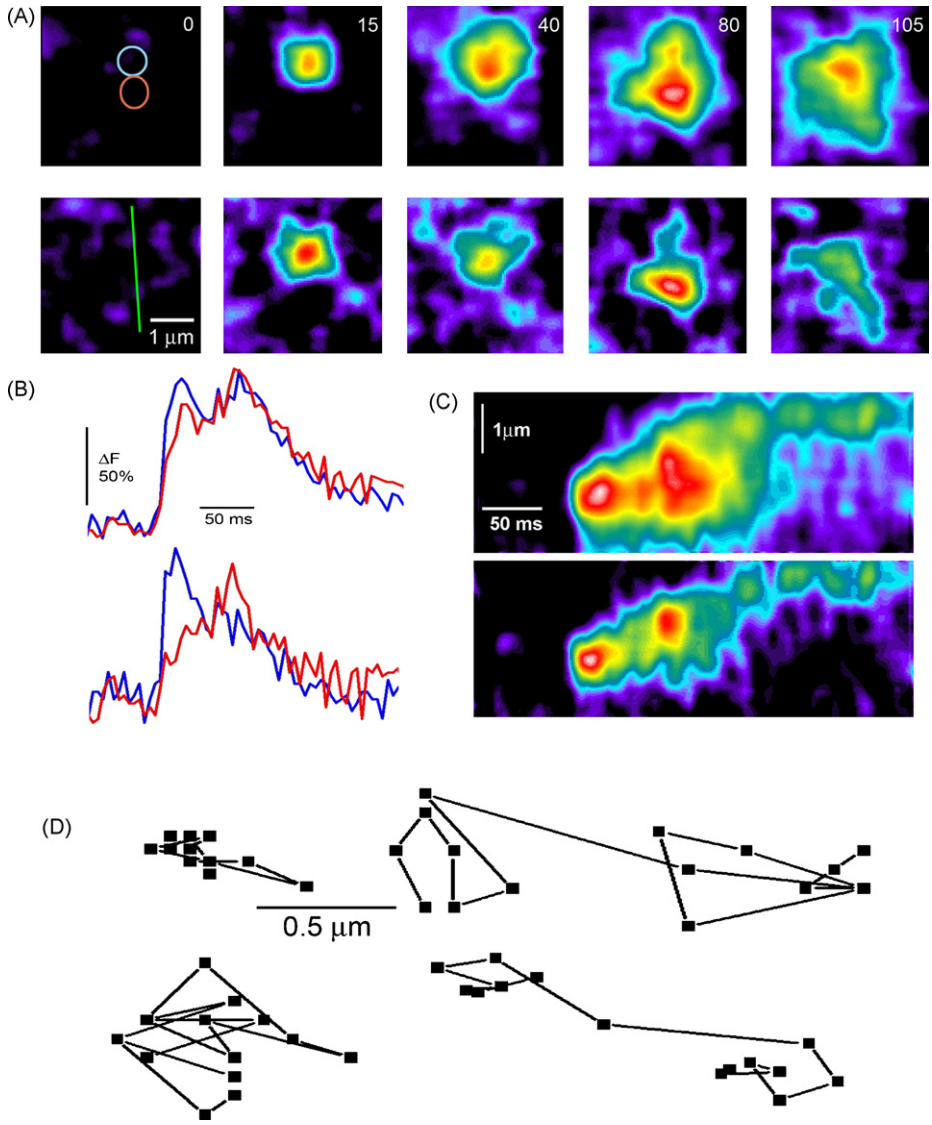

Fig. 5. 'Calcium deblurring' of multi-focal puff images. (A) The top image sequence shows the spatio-temporal evolution of a single puff, as captured by *Cam2*. Each panel is a single frame (5 ms integration time), acquired at times indicated in ms. The lower image sequence shows the same event after 'deblurring' by subtracting a smoothed average of frames acquired by *Cam1* and *Cam3* from the corresponding *Cam2* image. See Section 2 for further details. Colored circles in the top left frame indicate the regions of interest used to derive fluorescence profiles in (B), and the green line in the lower left frame marks the region used to derive the linescan images in (C). Increasing fluorescence ratio (increasing $[Ca^{2+}]$) is depicted on a pseudocolor rainbow scale, normalized separately in the raw and deblurred image sequences (but consistently within each sequence), with white corresponding to the greatest increase. (B) Temporal evolution of fluorescence signals measured from the two correspondingly colored circular regions (0.9 μm diameter) marked in (A). The top pair of traces were obtained from the upper, unprocessed *Cam2* image sequence and the lower pair from the deblurred sequence. (C) Linescan images depicting changes in fluorescence along the scan line marked in (A) derived from the raw *Cam2* images (top) and deblurred images (bottom). Note that the deblurred images (A and C) and profiles (B) clearly reveal that the puff involves two spatially and kinetically distinct sites of Ca^{2+} liberation, whereas this is barely evident in the unprocessed *Cam2* data. (D) Tracking the sites of Ca^{2+} release during puffs. Data are shown for 4 puffs arising at different sites in the same imaging record, and plots show the *x*–*y* coordinates of the centroid of the deblurred fluorescence signal at 5 ms increments throughout the durations of the puffs. The examples at the left are typical of 'stationary' puffs, whereas those at the right show 'jumping' puffs.

Cam2. We aim in future to extend the algorithm we had developed for deriving the dimensions and flux of underlying Ca^{2+} sources from linescan images [17] to the multi-dimensional data provided by 3-camera imaging. Nevertheless, the simple and computationally fast deblurring algorithm already effects a significant improvement, and comparison of processed images with the raw *Cam2* images reveals a sharper definition of the location and kinetics of the Ca^{2+} release flux underlying puffs (Fig. 5A: Supplementary Video#1, online). In particular, some puffs were seen to involve sequential Ca^{2+} release from two distinct sites (Fig. 5A–C: Supplementary Video#2, online), whereas they would have been interpreted to arise from a more sustained release from a single site based on conventional wide-field images. Tracking of the fluorescence centroid on deblurred images then enabled a mapping of the functional architecture of puff sites, with

Please cite this article in press as: A. Demuro, I. Parker, Multi-dimensional resolution of elementary Ca^{2+} signals by simultaneous multi-focal imaging, Cell Calc. (2007), doi:10.1016/j.ceca.2007.07.002

most showing only small (ca. ±200 nm) variations in release site that may simply reflect noise fluctuations (left panels, Fig. 5D), whereas a subset showed marked 'jumps' over several hundred nm. Functionally autonomous puff sites may not, therefore, be tightly grouped as an effective point source below the limit of microscopic resolution, as we had earlier proposed [15], but rather represent clusters or sub-clusters of IP_3 receptors distributed over several hundred nm across which Ca^{2+} 'nano-waves' propagate [18].

3.7. Conclusions

Multi-focal imaging with three high-speed cameras offers a straightforward method for 4-dimensional imaging of dynamic cellular processes with millisecond resolution. We demonstrate the potential of multi-focal imaging to resolve new features of local Ca^{2+} signaling events, and suggest that the technique should further be applicable to other fast dynamic intracellular processes, such as vesicle trafficking and fusion. The results presented here were obtained in a 1-week period when the cameras were generously loaned by the manufacturers, and we anticipate that the performance of the multi-focal system can be further enhanced by optimization of the optics and by development of dedicated software for image deconvolution. We are not aware of any other imaging modality that offers a similar combination of spatial resolution in three dimensions (albeit with only three planes in the *z*-axis) together with millisecond temporal resolution. Multi-focal imaging should thus provide a useful adjunct to optical sectioning techniques such as confocal, multiphoton and total internal reflection fluorescence (TIRF) microscopy. Although spinning-disc confocal microscopes provide similar time resolution, the problem remains of discriminating out-of focus events arising above or below the confocal section. Moreover, despite the cost of Cascade and similar electron-multiplied cameras, the total expense of a multi-focal microscope remains comparable to, or cheaper than even a basic confocal system.

Acknowledgements

We thank Roper Scientific for the generous loan of Cascade cameras. This work was supported by a grant (GM48071) from the National Institutes of Health.

Appendix A. Supplementary data

Supplementary data associated with this article can be found, in the online version, at doi:10.1016/j.ceca.2007.07.002.

References

[1] M.J. Berridge, Elementary and global aspects of calcium signaling, J. Physiol. 499 (1997) 291–306.
[2] I. Parker, J. Choi, Y. Yao, Elementary events of InsP_3-induced Ca^{2+} liberation in *Xenopus* oocytes: hot spot, puffs and blips, Cell Calcium 20 (1996) 105–121.
[3] N. Shirokova, A. Gonzalez, W.G. Kirsch, E. Rios, G. Pizarro, M.D. Stern, H. Cheng, Calcium sparks: release packets of uncertain origin and fundamental role, J. Gen. Physiol. 113 (1999) 373–376.
[4] Y.J. Yao, J. Choi, I. Parker, Quantal puffs of intracellular Ca^{2+} evoked by inositol triphosphate in *Xenopus* oocytes, J. Physiol. 482 (1995) 533–553.
[5] N. Callamaras, I. Parker, Construction of a line-scan confocal microscope for physiological recording, Methods Enzymol. 307 (1999) 152–169.
[6] V.R. Pratusevich, C.W. Balke, Factors shaping the confocal image of the calcium spark in cardiac muscle cells, Biophys. J. 71 (1996) 2942–2957.
[7] L.T. Izu, W.G. Wier, C.W. Balke, Theoretical analysis of the spark amplitude distribution, Biophys. J. 75 (1998) 1144–1162.
[8] M.T. Kirber, E.F. Etter, K.A. Bellve, L.M. Lifshitz, R.A. Tuft, F.S. Fay, J.V. Walsh, K.E. Fogarty, Relationship of Ca^{2+} sparks to STOCs studied with 2D and 3D imaging in feline esophageal smooth muscle cells, J. Physiol. 531 (2001) 315–317.
[9] H. Zou, L.M. Lifshitz, R.A. Tuft, K.E. Fogarty, J.J. Singer, Imaging calcium entering the cytosol through a single opening of plasma membrane ion channels: SCCaFTs—fundamental calcium events, Cell Calcium 35 (2004) 523–533.
[10] H. Zou, L.M. Lifshitz, R.A. Tuft, K.E. Fogarty, J.J. Singer, Using total fluorescence increase (signal mass) to determine the Ca^{2+} current underlying localized Ca^{2+} events, J. Gen. Physiol. 124 (2004) 259–272.
[11] D.L. Spector, R.D. Goldman, L.A. Leinwand, Confocal microscopy and deconvolution techniques, in: D.L. Spector, R.D. Goldman, L.A. Leinwand (Eds.), Cells: A Laboratory Manual, Light Microscopy and Cell Structure, vol. 2, Cold Spring Harbor Laboratory Press, Cold Spring Harbor, NY, 1998, pp. 96.1–96.23.
[12] A. Demuro, I. Parker, Optical single-channel recording: imaging Ca^{2+} flux through individual N-type voltage-gated channels expressed in *Xenopus* oocytes, Cell Calcium 34 (2003) 499–509.
[13] N. Callamaras, I. Parker, Phasic characteristic of elementary Ca^{2+} release sites underlying quantal responses to IP_3, EMBO J. 19 (2000) 3608–3617.
[14] S.L. Dargan, I. Parker, Buffer kinetics shape the spatiotemporal patterns of IP_3-evoked Ca^{2+} signals, J. Physiol. 553 (2003) 775–778.
[15] X.P. Sun, N. Callamaras, J.S. Marchant, I. Parker, A continuum of $InsP_3$-mediated elementary Ca^{2+} signaling events in *Xenopus* oocytes, J. Physiol. 509 (1998) 67–80.
[16] D. Thomas, P. Lipp, M.J. Berridge, M.D. Bootman, Hormone-evoked elementary Ca^{2+} signals are not stereotypic, but reflect activation of different size channel clusters and variable recruitment of channels within a cluster, J. Biol. Chem. 273 (1998) 27130–27136.
[17] A.C. Ventura, L. Bruno, A. Demuro, I. Parker, S.P. Dawson, A model-independent algorithm to derive Ca^{2+} fluxes underlying local cytosolic Ca^{2+} transients, Biophys. J. 88 (2005) 2403–2421.
[18] J. Shuai, H.J. Rose, I. Parker, The number and spatial distribution of IP_3 receptors underlying calcium puffs in *Xenopus* oocytes, Biophys. J. 91 (2006) 4033–4044.

Please cite this article in press as: A. Demuro, I. Parker, Multi-dimensional resolution of elementary Ca^{2+} signals by simultaneous multi-focal imaging, Cell Calc. (2007), doi:10.1016/j.ceca.2007.07.002